



Axisymmetric residual stresses in a solid cylinder of finite length

Lesya Postolaki · Yuriy Tokovyy

Received: 27 January 2022 / Accepted: 19 April 2022 / Published online: 18 May 2022
© The Author(s), under exclusive licence to Springer Nature B.V. 2022

Abstract A solution technique is presented for the determination of residual stresses in a finite-length solid cylinder subject to non-uniform axisymmetric distributions of incompatible residual strains. The problem is reduced to the sequential solving of three individual problems: a problem on the determination of residual stresses in an infinitely long cylinder (the basic state) and two auxiliary problems for evaluating the stresses induced by the end-face effects (the disturbed states). The variational method of homogeneous solutions is implemented in order to determine the disturbed states within the framework of two latter problems. The solution technique is verified numerically for typical distribution profiles of incompatible strains depending on both the radial and axial coordinates. The approach can be used to evaluate residual stresses in a solid cylinder of finite length due to the intense thermal treatment.

Keywords Axisymmetric elasticity · Finite-length solid cylinder · Homogeneous solutions · Residual stresses · Variational method

Mathematics Subject Classification 35J30 · 35J40 · 74B05 · 58E30

1 Introduction

The residual strains and stresses may occur in solids during various manufacturing processes, particularly welding, casting, high-pressure rolling, forming, etc. [1], and specific exploitation regimes quite often associated with intense non-uniform thermal impacts [2,3]. Being selfequilibrated, i.e., producing zero resultant force and moment within a macrovolume, the residual stresses are often neglected within the framework of the engineering estimates. Nevertheless, the impact of residual stresses, especially under the facilitating conditions, may peak the critical levels and cause structural failure [1,4].

L. Postolaki · Y. Tokovyy
Pidstryhach Institute for Applied Problems of Mechanics and Mathematics, National Academy of Sciences of Ukraine,
3-B Naukova St., Lviv 79060, Ukraine
e-mail: lesya.postolaki@gmail.com

Y. Tokovyy (✉)
Department of Applied Mathematics, Institute of Applied Mathematics and Fundamental Sciences, National University Lviv
Polytechnic, 5 Metropolita Andreia St., Lviv 79013, Ukraine
e-mail: tokovyy@gmail.com

The practical measurement of the residual strains or stresses in solids is typically based on either destructive or non-destructive testing. The destructive techniques imply the complete or partial destruction of structural members in order to perform the measurements (e.g., the hole drilling and ring coring techniques [5–7], the slitting and contour methods [8–10], etc.). On the other hand, the non-destructive methods (e.g., the X-ray and neutron diffraction [11–13], the magnetic, ultrasonic, and optical methods [14–16], etc.) allow for saving the structural integrity but have limited applicability. The most advanced way for predicting the actual levels of residual stresses corresponding to certain distribution profiles of incompatible strains combines both theoretical and experimental techniques [17, 18]. One of such approaches is a non-destructive computational–experimental method [19] based on solving the inverse elastoplastic problems [20] and fitting the results with the experimental evidence obtained by non-destructive techniques in order to evaluate the effective stress distribution parameters. The formulation and solution of the inverse problems is based on the so-called conventional-plastic strain hypothesis [21, 22] implying the base material of a solid to be elastic, while the expected zone of residual stress distribution exhibits specific elastic–plastic behavior so that the total strain can be represented in the following form:

$$\boldsymbol{\varepsilon} = \boldsymbol{\varepsilon}^e + \boldsymbol{\varepsilon}^0, \quad (1)$$

where $\boldsymbol{\varepsilon}$ is the total strain tensor, $\boldsymbol{\varepsilon}^e$ is the tensor of elastic strains occurring within the entire solid, and $\boldsymbol{\varepsilon}^0$ denotes the tensor of incompatible strain [23] distributed within the area affected by the impacts causing the residual stress–strain state. This approach has been efficiently employed for the analysis of residual stresses due to welding residual strains in infinite layers with rectilinear and circular welds [24, 25], butt-welded cylindrical vessels [26, 27], and rectangular plates [28]. Special attention in the latter paper was given to the end effects in the butt-welded rectangular plate by performing the exact analysis based on the direct integration method [29]. It was shown, in particular, that the presence of boundary that is transverse to the butt-weld axis effects significantly the aggregated stress state comparing with one for an infinitely long (with respect to the butt-weld length) plate. Thus, the end effects are very important for the accuracy in the evaluation of the residual stress–strain state of the bounded domains.

In general, the exact analysis of the end effects in the stress state of finite solids with irregular points (lines) of the boundary (i.e., the corner points or the edge lines) presents a challenge for both analytical and numerical methods due to the fact that the resulting operator of the corresponding boundary value problem of the elasticity theory is not self-conjugated. This fact complicates significantly the variables separation in the governing equations and, consequently, exact satisfaction on the boundary conditions imposed on the dissimilar segments of the boundary separated with the corner points. An interested reader can find more detail on the earlier development history of the methods for two-dimensional problems of such kind presented by Meleshko [30].

In the case of general boundary conditions, the dominant analytical methods for solving the boundary value problems for finite domains with corner points imply the realization of one of the following strategies: *A*) the construction of general solutions to the governing equations which allow for approximate satisfaction of boundary conditions imposed on some or all sides of a finite domain, and *B*) the construction of a solution that exactly satisfies the full set of boundary conditions imposed, while the governing equations are satisfied within the required accuracy. Strategy *B* was realized, for example, with the method of direct integration [29, 31], which has been recently used in [32] for solving a thermoelasticity problem in a cylinder of finite length. Strategy *A* is represented by at least two dominant methods, i.e., the method of cross-wise superposition [33, 34] and the method of homogeneous solutions [35]. The latter method presents a natural extension of the classical separation of variables implying the construction of eigenvalues, which belong to the complex plane \mathbb{C} in the case of finite domains with corner points. The corresponding eigenfunctions are usually non-orthogonal which complicates the satisfaction of boundary conditions. In order to overcome this difficulty, the variational approaches with implication of the least square method are often employed. In [36], a variational method of homogeneous solutions was used for the evaluation of residual stresses in the vicinity of an inplane weld joint connecting the dissimilar materials. This method was also used for the solution of problems on the non-destructive evaluation of the axisymmetric residual stresses near circular welds in long cylindrical shells on the basis of the available empirical data obtained through the magnetoelastic method [37].

A variational method of homogeneous solutions was used in [38,39] for the analysis of axisymmetric residual stresses in a finite-length cylinder. The residual stresses are modeled with the use of concept of incompatible residual strains (1) with the latter strains being regarded as the cause of the residual stresses appearance. The incompatible strains were presented by an isotropic tensor depending only on the radial coordinate. This method was also used for a variational formulation of the inverse problem for the residual stresses determination on the basis of empirical data obtained by a photoelasticity method. This paper is aimed to extend the technique on the evaluation of the axisymmetric residual stresses in a finite-length solid cylinder due to the incompatible strains depending on both the radial and axial coordinates. This provides a prominent tool for the analysis of the end effects in the cylinders of finite length.

2 Mathematical formulation of the problem

Consider an elastic cylinder of finite length $2H$ and radius R . In the dimensionless cylindrical coordinate system, the cylinder occupies domain $\mathcal{C} = \{(r, \theta, z) : r \in [0, 1], \theta \in [0, 2\pi], z \in [-b, b]\}$. Here, $r = \rho/R$, $z = \zeta/R$, $b = H/R$, ρ and ζ are the dimensional radial and axial coordinates, and θ is the circumferential coordinate. Assume the lateral surface and the end faces of the cylinder to be free of the external force loadings, i.e.,

$$\sigma_{rr}(1, z) = \sigma_{rz}(1, z) = 0, \quad \sigma_{zz}(r, \pm b) = \sigma_{rz}(r, \pm b) = 0. \tag{2}$$

Here, $\sigma_{rr}(r, z)$, $\sigma_{zz}(r, z)$, and $\sigma_{rz}(r, z)$ are the normal and tangential stress-tensor components.

Assume the interior of the cylinder to undergo a non-uniform axisymmetric (i.e., irrespective of coordinate θ) distribution of incompatible [23] strains $\varepsilon_{rr}^0(r, z)$, $\varepsilon_{\theta\theta}^0(r, z)$, and $\varepsilon_{zz}^0(r, z)$ induced by thermal treatment and, hence, represented by the normal components only [40]. Then, according to the model (1), the components $\varepsilon_{rr}(r, z)$, $\varepsilon_{\theta\theta}(r, z)$, $\varepsilon_{zz}(r, z)$, and $\varepsilon_{rz}(r, z)$ of the total strain are to be represented in the form as follows:

$$\begin{aligned} \varepsilon_{rr}(r, z) &= \varepsilon_{rr}^e(r, z) + \varepsilon_{rr}^0(r, z), & \varepsilon_{\theta\theta}(r, z) &= \varepsilon_{\theta\theta}^e(r, z) + \varepsilon_{\theta\theta}^0(r, z), \\ \varepsilon_{zz}(r, z) &= \varepsilon_{zz}^e(r, z) + \varepsilon_{zz}^0(r, z), & \varepsilon_{rz}(r, z) &= \varepsilon_{rz}^e(r, z). \end{aligned} \tag{3}$$

Here, $\varepsilon_{rr}^e(r, z)$, $\varepsilon_{zz}^e(r, z)$, $\varepsilon_{\theta\theta}^e(r, z)$, and $\varepsilon_{rz}^e(r, z)$ are the elastic strains.

The total strains are expressed through the radial and axial displacements, $u_r(r, z)$ and $u_z(r, z)$, via the strain-displacement Cauchy equations [41]:

$$\begin{aligned} \varepsilon_{rr}(r, z) &= \frac{\partial u_r(r, z)}{\partial r}, & \varepsilon_{\theta\theta}(r, z) &= \frac{u_r(r, z)}{r}, \\ \varepsilon_{zz}(r, z) &= \frac{\partial u_z(r, z)}{\partial z}, & \varepsilon_{rz}(r, z) &= \frac{1}{2} \left(\frac{\partial u_r(r, z)}{\partial z} + \frac{\partial u_z(r, z)}{\partial r} \right). \end{aligned} \tag{4}$$

Within the context of equations (3) and (4), the constitutive equations of Hooke’s law [40,41] take the following form:

$$\begin{aligned} \sigma_{rr}(r, z) &= \lambda\varepsilon(r, z) + 2\mu \frac{\partial u_r(r, z)}{\partial r} - \lambda\varepsilon_0(r, z) - 2\mu\varepsilon_{rr}^0(r, z), \\ \sigma_{\theta\theta}(r, z) &= \lambda\varepsilon(r, z) + 2\mu \frac{u_r(r, z)}{r} - \lambda\varepsilon_0(r, z) - 2\mu\varepsilon_{\theta\theta}^0(r, z), \\ \sigma_{zz}(r, z) &= \lambda\varepsilon(r, z) + 2\mu \frac{\partial u_z(r, z)}{\partial z} - \lambda\varepsilon_0(r, z) - 2\mu\varepsilon_{zz}^0(r, z), \\ \sigma_{rz}(r, z) &= \mu \left(\frac{\partial u_r(r, z)}{\partial z} + \frac{\partial u_z(r, z)}{\partial r} \right), \end{aligned} \tag{5}$$

where $\varepsilon = \partial u_r/\partial r + u_r/r + \partial u_z/\partial z$, $\varepsilon_0 = \varepsilon_{rr}^0 + \varepsilon_{\theta\theta}^0 + \varepsilon_{zz}^0$, and λ and μ are the Lamé constants.

Assuming the cylinder to be in the state of equilibrium, the stress-tensor components meet the following equilibrium equations [40,41]

$$\begin{aligned} \frac{1}{r} \frac{\partial(r\sigma_{rr}(r, z))}{\partial r} + \frac{\partial\sigma_{rz}(r, z)}{\partial z} - \frac{\sigma_{\theta\theta}(r, z)}{r} &= 0, \\ \frac{1}{r} \frac{\partial(r\sigma_{rz}(r, z))}{\partial r} + \frac{\partial\sigma_{zz}(r, z)}{\partial z} &= 0. \end{aligned} \tag{6}$$

Substituting equations (5) into the equilibrium equations (6) yields the following Lamé–Navier equations:

$$\begin{aligned} \mu \left(\nabla^2 u_r(r, z) - \frac{u_r(r, z)}{r^2} \right) + (\lambda + \mu) \frac{\partial \varepsilon(r, z)}{\partial r} &= f(r, z), \\ \mu \nabla^2 u_z(r, z) + (\lambda + \mu) \frac{\partial \varepsilon(r, z)}{\partial z} &= g(r, z), \end{aligned} \quad (7)$$

where

$$\begin{aligned} f(r, z) &= \frac{\partial}{\partial r} \left(\lambda \varepsilon_0(r, z) + 2\mu \varepsilon_{rr}^0(r, z) \right) + \frac{2\mu}{r} \left(\varepsilon_{rr}^0(r, z) - \varepsilon_{\theta\theta}^0(r, z) \right), \\ g(r, z) &= \frac{\partial}{\partial z} \left(\lambda \varepsilon_0(r, z) + 2\mu \varepsilon_{zz}^0(r, z) \right), \quad \nabla^2 = \frac{\partial^2}{\partial r^2} + \frac{1}{r} \frac{\partial}{\partial r} + \frac{\partial^2}{\partial z^2}. \end{aligned}$$

For the case of isotropic tensor of incompatible strains, i.e., when $\varepsilon_{rr}^0 = \varepsilon_{\theta\theta}^0 = \varepsilon_{zz}^0 = \varepsilon_0/3$, Eqs. (7) take the following form:

$$\begin{aligned} \mu \left(\nabla^2 u_r(r, z) - \frac{u_r(r, z)}{r^2} \right) + (\lambda + \mu) \frac{\partial \varepsilon(r, z)}{\partial r} &= \frac{\partial \eta(r, z)}{\partial r}, \\ \mu \nabla^2 u_z(r, z) + (\lambda + \mu) \frac{\partial \varepsilon(r, z)}{\partial z} &= \frac{\partial \eta(r, z)}{\partial z}, \end{aligned} \quad (8)$$

where $\eta = (3\lambda + 2\mu)\varepsilon_0/3$.

Equations (2)–(5) and (8) present a mathematical model (a closed-form boundary value problem) for the determination of axisymmetric residual stresses and displacements in cylinder \mathcal{C} due to non-uniform distributions of incompatible strains represented with the isotropic tensor induced by intensive thermal treatment depending on both the radial and axial coordinates. Below, we provide a solution technique for the formulated problem based on the variational method of homogeneous solutions.

3 Solution technique

3.1 Solution structure

In our approach, we follow the solution strategy [39] by presenting the displacement field as a superposition of two states, i.e.,

$$u_r(r, z) = \hat{u}_r(r, z) + \tilde{u}_r(r, z), \quad u_z(r, z) = \hat{u}_z(r, z) + \tilde{u}_z(r, z).$$

Here, $\hat{u}_r(r, z)$ and $\hat{u}_z(r, z)$ are the displacements resulted from non-homogeneous equations (8) for an infinitely long cylinder ($b^2 \rightarrow \infty$) of the unit radius (they reflect the so-called basic state of the cylinder), and $\tilde{u}_r(r, z)$ and $\tilde{u}_z(r, z)$ are the displacements derived from the corresponding homogeneous equations

$$\begin{aligned} \mu \left(\nabla^2 \tilde{u}_r(r, z) - \frac{\tilde{u}_r(r, z)}{r^2} \right) + (\lambda + \mu) \frac{\partial \tilde{\varepsilon}(r, z)}{\partial r} &= 0, \\ \mu \nabla^2 \tilde{u}_z(r, z) + (\lambda + \mu) \frac{\partial \tilde{\varepsilon}(r, z)}{\partial z} &= 0, \end{aligned} \quad (9)$$

formulated for cylinder \mathcal{C} . Here, $\tilde{\varepsilon} = \partial \tilde{u}_r / \partial r + \tilde{u}_r / r + \partial \tilde{u}_z / \partial z$. The latter displacements reflect the disturbance of the deformed state due to the end effects and thus are referred to as the “disturbed state.”

3.2 Basic state

In order to construct a solution to the system of non-homogeneous equations (8) for the basic state, we implement the following representation [33]:

$$\hat{u}_r(r, z) = \frac{\partial \Phi(r, z)}{\partial r}, \quad \hat{u}_z(r, z) = \frac{\partial \Phi(r, z)}{\partial z}, \quad (10)$$

where $\Phi(r, z)$ is an unknown potential function that is analogous to the Papkovitch – Goodier thermoelastic potential [42,43].

Substitution of representations (10) into (8) yields

$$\nabla^2 \Phi(r, z) = -4\pi\omega(r, z), \quad \omega(r, z) = -\frac{1}{\lambda + 2\mu} \frac{\eta(r, z)}{4\pi}. \tag{11}$$

A solution to Eq. (11) can be given in the form as follows [44]:

$$\Phi(r, z) = \iint_{\mathcal{C}} \mathcal{G}(r, z; \xi, \zeta) \omega(\xi, \zeta) \xi \, d\xi \, d\zeta, \tag{12}$$

where

$$\mathcal{G}(r, z; \xi, \zeta) = \frac{\mathcal{K}(m)}{\pi \sqrt{(r + \xi)^2 + (z - \zeta)^2}},$$

$$m \equiv m(r, z; \xi, \zeta) = \frac{4r\xi}{(r + \xi)^2 + (z - \zeta)^2},$$

$\mathcal{K}(m)$ is the Legendre complete normal elliptic integral of the first kind

$$\mathcal{K}(m) = \int_0^1 \frac{dt}{\sqrt{(1-t^2)(1-t^2m^2)}}, \quad \mathcal{K}(0) = \frac{\pi}{2}, \quad \mathcal{K}(1) = \infty,$$

which can be evaluated by making use of the following formula:

$$\mathcal{K}(m) = \frac{\pi}{2} \sum_{k=0}^{\infty} \frac{(2k)!}{2^{2k} (k!)^2} m^{2k}.$$

Thus, the displacements $\hat{u}_r(r, z)$ and $\hat{u}_z(r, z)$ can be computed by putting (12) into (10). The corresponding stress-tensor components, $\hat{\sigma}_{rr}(r, z)$, $\hat{\sigma}_{\theta\theta}(r, z)$, $\hat{\sigma}_{zz}(r, z)$, and $\hat{\sigma}_{rz}(r, z)$, can be computed by making use of (5), (10), and (11) in the following form:

$$\hat{\sigma}_{rr}(r, z) = 2\mu \left(\frac{\partial^2 \Phi(r, z)}{\partial r^2} - \frac{1}{\lambda + 2\mu} \eta(r, z) \right),$$

$$\hat{\sigma}_{\theta\theta}(r, z) = 2\mu \left(\frac{1}{r} \frac{\partial \Phi(r, z)}{\partial r} - \frac{1}{\lambda + 2\mu} \eta(r, z) \right),$$

$$\hat{\sigma}_{zz}(r, z) = 2\mu \left(\frac{\partial^2 \Phi(r, z)}{\partial z^2} - \frac{1}{\lambda + 2\mu} \eta(r, z) \right),$$

$$\hat{\sigma}_{rz}(r, z) = 2\mu \frac{\partial^2 \Phi(r, z)}{\partial r \partial z}.$$

In such manner, the stresses and displacements are determined for the basic state of an infinitely long solid elastic cylinder of the unit radius under the isotropic incompatible strains distributed non-uniformly within the coordinates (r, z) . These components induce the non-uniform boundary conditions on the lateral surface and the end faces of the finite cylinder \mathcal{C} . In order to compensate these non-uniform boundary conditions, we introduce the “disturbed state,” which can be determined by implementing the technique presented in the following section.

3.3 Disturbed state

The disturbed state is to be realized by solving the following two boundary value problems.

The first problem implies solving system (9) for cylinder \mathcal{C} with free lateral surface

$$\hat{\sigma}_{rr}^{(1)}(1, z) = 0, \quad \hat{\sigma}_{rz}^{(1)}(1, z) = 0, \tag{13}$$

and the end faces loaded as follows:

$$\tilde{\sigma}_{zz}^{(1)}(r, \pm b) = -\hat{\sigma}_{zz}(r, \pm b), \quad \tilde{\sigma}_{rz}^{(1)}(r, \pm b) = \hat{\sigma}_{rz}(r, \pm b). \tag{14}$$

The second boundary value problem implies solving the system (9) accompanied with the boundary conditions of free end faces

$$\tilde{\sigma}_{zz}^{(2)}(r, \pm b) = 0, \quad \tilde{\sigma}_{rz}^{(2)}(r, \pm b) = 0 \tag{15}$$

along with the conditions of loaded lateral surface

$$\tilde{\sigma}_{rr}^{(2)}(1, z) = -\hat{\sigma}_{rr}(1, z), \quad \tilde{\sigma}_{rz}^{(2)}(1, z) = -\hat{\sigma}_{rz}(1, z). \tag{16}$$

The total components for the disturbed state can be computed by superposing the solutions of boundary value problems (9), (13), and (14), and (9), (15), and (16).

A general solution to system (9) can be constructed by implementing the Love stress function $\chi(r, z)$ [45] satisfying the following biharmonic equation

$$\nabla^2 \nabla^2 \chi(r, z) = 0.$$

The displacements are represented via the Love function by the following expressions:

$$\tilde{u}_r(r, z) = -\frac{\partial^2 \chi(r, z)}{\partial r \partial z}, \quad \tilde{u}_z(r, z) = 2(1 - \nu) \nabla^2 \chi(r, z) + \frac{\partial^2 \chi(r, z)}{\partial z^2},$$

and the stress-tensor components are expressed as follows:

$$\begin{aligned} \tilde{\sigma}_{rr}(r, z) &= 2\mu \frac{\partial}{\partial z} \left(\nu \nabla^2 \chi(r, z) - \frac{\partial^2 \chi(r, z)}{\partial r^2} \right), \\ \tilde{\sigma}_{\theta\theta}(r, z) &= 2\mu \frac{\partial}{\partial z} \left(\nu \nabla^2 \chi(r, z) - \frac{1}{r} \frac{\partial \chi(r, z)}{\partial r} \right), \\ \tilde{\sigma}_{zz}(r, z) &= 2\mu \frac{\partial}{\partial z} \left((2 - \nu) \nabla^2 \chi(r, z) - \frac{\partial^2 \chi(r, z)}{\partial z^2} \right), \\ \tilde{\sigma}_{rz}(r, z) &= 2\mu \frac{\partial}{\partial r} \left((1 - \nu) \nabla^2 \chi(r, z) - \frac{\partial^2 \chi(r, z)}{\partial z^2} \right). \end{aligned} \tag{17}$$

Here, ν is the Poisson ratio.

In view of the linearity of the problem, we can construct the Love functions $\chi^{(1)}(r, z)$ and $\chi^{(2)}(r, z)$ corresponding to the boundary value problems (9), (13), (14) and (9), (15), (16), separately; then they can be superposed in order to determine the disturbed stress–strain state of the finite cylinder \mathcal{C} .

Assuming, for the simplicity sake, the symmetry of the problem with respect to the plane $z = 0$, we can represent function $\chi^{(1)}(r, z)$ in the following form [46]:

$$\chi^{(1)}(r, z) = \frac{1}{2} \sum_{k=1}^{\infty} (B_k \cosh(\gamma_k z) f_k(r) + \bar{B}_k \cosh(\bar{\gamma}_k z) \bar{f}_k(r)), \tag{18}$$

where B_k are unknown complex constants, the overline denotes the complex conjugation,

$$f_k(r) = r \kappa_k J_1(\gamma_k r) - \frac{2}{\pi \gamma_k} J_0(\gamma_k r),$$

γ_k are the complex roots of the transcendental characteristic equation

$$\gamma_k^2 \left(J_0^2(\gamma_k) + J_1^2(\gamma_k) \right) - 2(1 - \nu) J_1^2(\gamma_k) = 0,$$

$$\kappa_k = -\frac{2}{\pi} \frac{J_1(\gamma_k)}{2(1 - \nu) J_1(\gamma_k) + \gamma_k J_0(\gamma_k)}.$$

Within the context of expressions (17) and (18), the stress field for the first disturbed problem (9), (13), and (14) can be given in the form as follows:

$$\begin{aligned}
 \tilde{\sigma}_{rr}^{(1)}(r, z) &= \frac{1}{2} \sum_{k=1}^{\infty} \left(B_k \sigma_{rr,k}^{(1)}(r, z) + \bar{B}_k \bar{\sigma}_{rr,k}^{(1)}(r, z) \right), \\
 \tilde{\sigma}_{\theta\theta}^{(1)}(r, z) &= \frac{1}{2} \sum_{k=1}^{\infty} \left(B_k \sigma_{\theta\theta,k}^{(1)}(r, z) + \bar{B}_k \bar{\sigma}_{\theta\theta,k}^{(1)}(r, z) \right), \\
 \tilde{\sigma}_{zz}^{(1)}(r, z) &= \frac{1}{2} \sum_{k=1}^{\infty} \left(B_k \sigma_{zz,k}^{(1)}(r, z) + \bar{B}_k \bar{\sigma}_{zz,k}^{(1)}(r, z) \right), \\
 \tilde{\sigma}_{rz}^{(1)}(r, z) &= \frac{1}{2} \sum_{k=1}^{\infty} \left(B_k \sigma_{rz,k}^{(1)}(r, z) + \bar{B}_k \bar{\sigma}_{rz,k}^{(1)}(r, z) \right),
 \end{aligned} \tag{19}$$

where $\sigma_{rr,k}^{(1)}(r, z)$, $\sigma_{\theta\theta,k}^{(1)}(r, z)$, $\sigma_{zz,k}^{(1)}(r, z)$, and $\sigma_{rz,k}^{(1)}(r, z)$ are given in Appendix A. Expressions (19) allow for exact satisfaction of the equations in system (9) and boundary conditions (13) under arbitrary constants B_k , which are to be found by satisfying conditions (14).

The biharmonic function for the second disturbed problem $\chi^{(2)}(r, z)$ can be constructed in the form as follows [47]:

$$\chi^{(2)}(r, z) = \frac{1}{2} \sum_{k=1}^{\infty} \left(A_k \varphi_k(z) J_0(\lambda_k r) + \bar{A}_k \bar{\varphi}_k(z) J_0(\bar{\lambda}_k r) \right), \tag{20}$$

where $\varphi_k(z) = \varkappa_k \sinh(\lambda_k z) + z \cosh(\lambda_k z)$, $\varkappa_k = -2\nu/\lambda_k - b/\tanh(\lambda_k b)$, and λ_k are the complex roots of the transcendental characteristic equation $\sinh(2\lambda_k b) + 2\lambda_k b = 0$.

Now, using (17) and (20), we can construct the stresses for the second disturbed problem (9), (15), and (16) in the following form:

$$\begin{aligned}
 \tilde{\sigma}_{rr}^{(2)}(r, z) &= \frac{1}{2} \sum_{k=1}^{\infty} \left(A_k \sigma_{rr,k}^{(2)}(r, z) + \bar{A}_k \bar{\sigma}_{rr,k}^{(2)}(r, z) \right) + c, \\
 \tilde{\sigma}_{\theta\theta}^{(2)}(r, z) &= \frac{1}{2} \sum_{k=1}^{\infty} \left(A_k \sigma_{\theta\theta,k}^{(2)}(r, z) + \bar{A}_k \bar{\sigma}_{\theta\theta,k}^{(2)}(r, z) \right), \\
 \tilde{\sigma}_{zz}^{(2)}(r, z) &= \frac{1}{2} \sum_{k=1}^{\infty} \left(A_k \sigma_{zz,k}^{(2)}(r, z) + \bar{A}_k \bar{\sigma}_{zz,k}^{(2)}(r, z) \right), \\
 \tilde{\sigma}_{rz}^{(2)}(r, z) &= \frac{1}{2} \sum_{k=1}^{\infty} \left(A_k \sigma_{rz,k}^{(2)}(r, z) + \bar{A}_k \bar{\sigma}_{rz,k}^{(2)}(r, z) \right).
 \end{aligned} \tag{21}$$

Here, functions $\sigma_{rr,k}^{(2)}(r, z)$, $\sigma_{\theta\theta,k}^{(2)}(r, z)$, $\sigma_{zz,k}^{(2)}(r, z)$, and $\sigma_{rz,k}^{(2)}(r, z)$ are given in Appendix B, and c is an arbitrary constant.

Representations (19) of the stress-tensor components meet the boundary conditions (13) under arbitrary coefficients B_k . Meanwhile, representations (21) meet the boundary conditions in (15) under arbitrary coefficients A_k . Obviously, the sets of coefficients B_k and A_k , $k = 1, 2, \dots$, can be determined by satisfying conditions (14) with expressions (19) and conditions (16) with expressions (21), respectively. In order to do so, we implement the variational method of homogeneous solutions [39] by introducing the following quadratic functionals corresponding to the first and second disturbed problems:

$$\mathcal{F}_1 = \int_0^1 r \left(\left(\tilde{\sigma}_{zz}^{(1)}(r, \pm b) + \hat{\sigma}_{zz}(r, \pm b) \right)^2 + \left(\tilde{\sigma}_{rz}^{(1)}(r, \pm b) + \hat{\sigma}_{rz}(r, \pm b) \right)^2 \right) dr, \tag{22}$$

$$\mathcal{F}_2 = \int_0^b \left(\left(\tilde{\sigma}_{rr}^{(2)}(1, z) + \hat{\sigma}_{rr}(1, z) \right)^2 + \left(\tilde{\sigma}_{rz}^{(2)}(1, z) + \hat{\sigma}_{rz}(1, z) \right)^2 \right) dz. \tag{23}$$

The functionals in (22) and (23) can be minimized under the following necessary conditions [48]:

$$\frac{\partial \mathcal{F}_1}{\partial B_k} = 0, \quad \frac{\partial \mathcal{F}_1}{\partial \bar{B}_k} = 0, \quad \frac{\partial \mathcal{F}_2}{\partial A_k} = 0, \quad \frac{\partial \mathcal{F}_2}{\partial \bar{A}_k} = 0, \quad \frac{\partial \mathcal{F}_2}{\partial c} = 0. \tag{24}$$

The last equation in (24) yields the following formula:

$$c = -\frac{1}{4b} \int_0^b \sum_{k=1}^{\infty} \left(A_k \sigma_{rr,k}^{(2)}(r, z) + \bar{A}_k \bar{\sigma}_{rr,k}^{(2)}(r, z) \right) dz.$$

Within the context of the latter formula along with the representations (14), (16), (19), and (21) the remaining equations in (24) yield the following infinite systems of linear algebraic equations:

$$\sum_{k=1}^{\infty} \sum_{p=1}^2 M_{mk}^{lp} B_k^p = K_m^l, \quad \sum_{k=1}^{\infty} \sum_{p=1}^2 N_{mk}^{lp} A_k^p = L_m^l, \tag{25}$$

where $B_k^1 = B_k, B_k^2 = \bar{B}_k, A_k^1 = A_k, A_k^2 = \bar{A}_k$, and the coefficients $M_{mk}^{lp}, N_{mk}^{lp}, K_m^l$, and $L_m^l, l = 1, 2, m = 1, 2, p = 1, 2$, and $k = 1, 2, \dots$, are given in Appendix C.

In view of the zero asymptotic of the coefficients in the systems given by equation (25) at $k \rightarrow \infty$, the practical computation of the parameters A_k^p and B_k^p along with their complex conjugation can be performed by implementing the simple reduction algorithm [48].

The total values of the stress-tensor components of the first and second disturbed problems and the stress components of the initial state are the solution of the formulated direct problem of determining the residual stresses.

4 Numerical examples and discussion

Consider a numerical example of the isotropic tensor of residual strain given by formula

$$\varepsilon_0(r, z) = \frac{1}{2} \begin{cases} e_1 \text{Fa} \left(a_r, -r + \frac{r_1}{2} \right) \\ \quad \times \left(1 - \text{Fa}(a_z, -b_1 + z) - \text{Fa}(a_z, -b_1 - z) \right), & 0 \leq r < r_1, \\ 0, & r_1 \leq r \leq r_2, \\ e_2 \text{Fa} \left(a_r, r - \frac{1+r_2}{2} \right) \\ \quad \times \left(1 - \text{Fa}(a_z, -b_1 + z) - \text{Fa}(a_z, -b_1 - z) \right), & r_2 < r \leq b. \end{cases} \tag{26}$$

Here, $\text{Fa}(a, x) = (\tanh(ax) + 1)/2, a = \{a_r, a_z\}, e_l, r_l$, and b_1 are given constant parameters, $l = 1, 2$. Figure 1 presents the distribution of the residual strain (26) computed under the fixed parameters $e_1 = 1, e_2 = -1, r_1 = 1/3, r_2 = 2/3, b = 1, a_r = 18, a_z = 10$, and four different values $b_1 = 1.00; 0.75; 0.50; 0.25$. Note that the strain ε_0 given in the form (26) varies within both the radial and axial coordinates, r and z . It reflects extension on the cylinder axis, which is maximum at $z = 0$ and decreases when approaching the end faces $z = \pm b$. On the lateral surface of the cylinder, the strain (26) verbalizes contraction which decreases when approaching the end faces. For smaller positive values of b_1 , the decrement occurs faster. The area $r_1 < r < r_2$, whose width is defined by $r_2 - r_1$, is not disturbed with the residual strain (26). Thus, by controlling the parameters involved in (26), it is possible

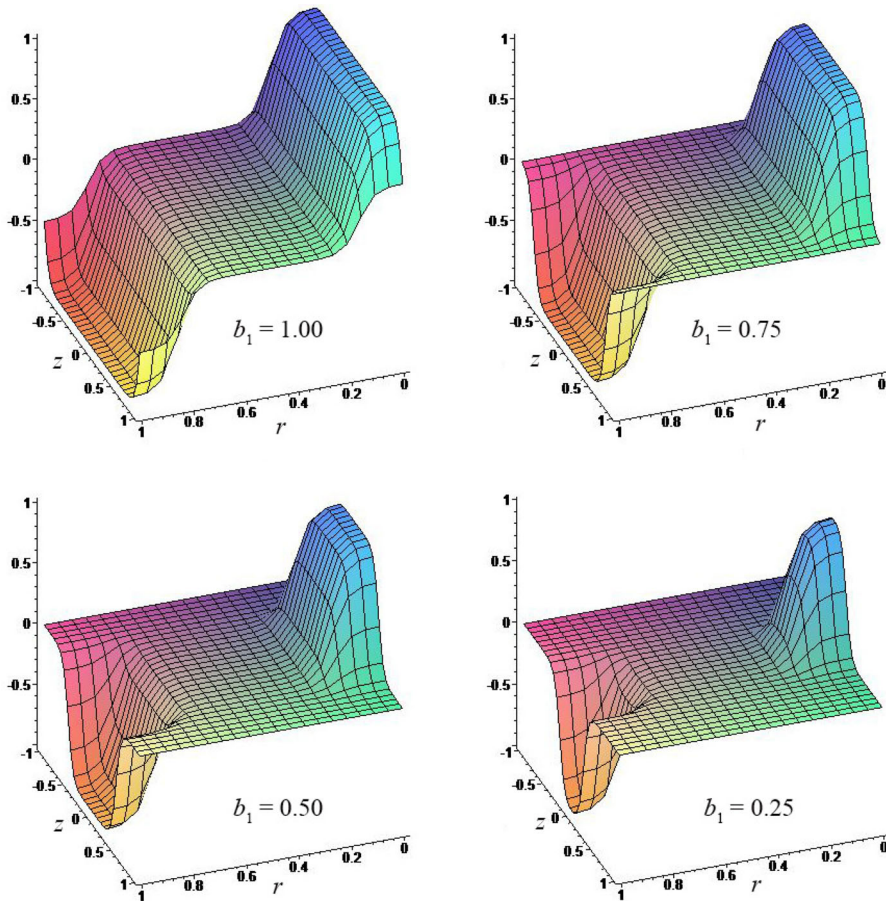


Fig. 1 Full-field distributions of the residual strain (26) in a “cubic” cylinder (the radius equals the half-length) at $e_1 = 1, e_2 = -1, r_1 = 1/3, r_2 = 2/3, b = 1, a_r = 18, a_z = 10,$ and $b_1 = 1.00; 0.75; 0.50; 0.25$

to control the distribution profile and the magnitude of the residual stress ε_0 . Note that decreasing the value of b_1 allows for reflecting rather “localized” effect of the residual strain (26) at a distance from the cylinder’s end faces. So that for small values of b_1 , the cylinder can be regarded as an infinitely long. On the contrary, the greater values of b_1 allow for capturing the end effects in the distribution of residual stresses due to the strain (26).

Figures 2–5 present the plots for the radial, axial, circumferential, and tangential stresses in a “cuboid” cylinder \mathcal{C} (i.e., the one with ratio equal to one, $b = 1$) due to the residual strain (26) computed under the following parameters: $e_1 = 1, e_2 = -1, r_1 = 1/3, r_2 = 2/3, b = 1, a_r = 18, a_z = 10$. The Poisson ratio in all considered case studies is $\nu = 0.3$. In the figures, curves 1–5 correspond to the values $r = 0; 1/6; 1/2; 5/6; 1$, respectively, indicating the axis, cylindrical midsurface and lateral surface of the cylinder, as well as the middles of the disturbed zones. The solutions of systems in (25) were computed through the simple reduction algorithm by holding $N = 15$ terms in the sums by k .

As we can observe in Fig. 2, the computed radial stress exactly satisfies the boundary condition (2) on the lateral surface (curves 5) under all the considered distribution profiles of the residual strain (26). For $b_1 = 0.25$, and smaller, the stress exhibits the trend typical for the distributions in infinitely long cylinder, i.e., tending to zero at cross-sections $z = \text{const}$, which are far enough from the plane $z = 0$. The magnitude of the residual radial stress at the cylinder axis decreases with decrement of b_1 . For the greater values of b_1 , curves 3 and 4 are remarkably close to one another. However, for the case studies of lesser end-effect, i.e., for $b_1 = 0.25$, the difference between the radial stress at these radii is more pronounced at $z = 0$. Quite similar behavior is observed in the circumferential

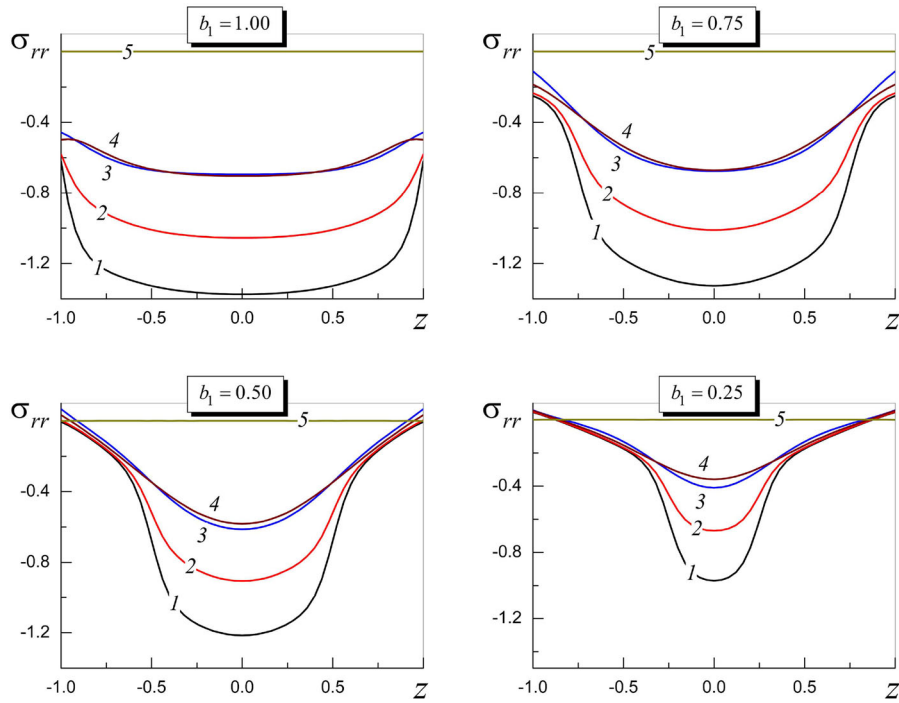


Fig. 2 The radial stress versus axial coordinate z at the specific radii $r = 0$ (curve 1), $r = 1/6$ (curve 2), $r = 1/2$ (curve 3), $r = 5/6$ (curve 4), and $r = 1$ (curve 5) of a “cubic” cylinder \mathcal{C} under the residual strains given by (26), where $e_1 = 1$, $e_2 = -1$, $r_1 = 1/3$, $r_2 = 2/3$, $b = 1$, $a_r = 18$, $a_z = 10$, and $b_1 = 1.00; 0.75; 0.50; 0.25$

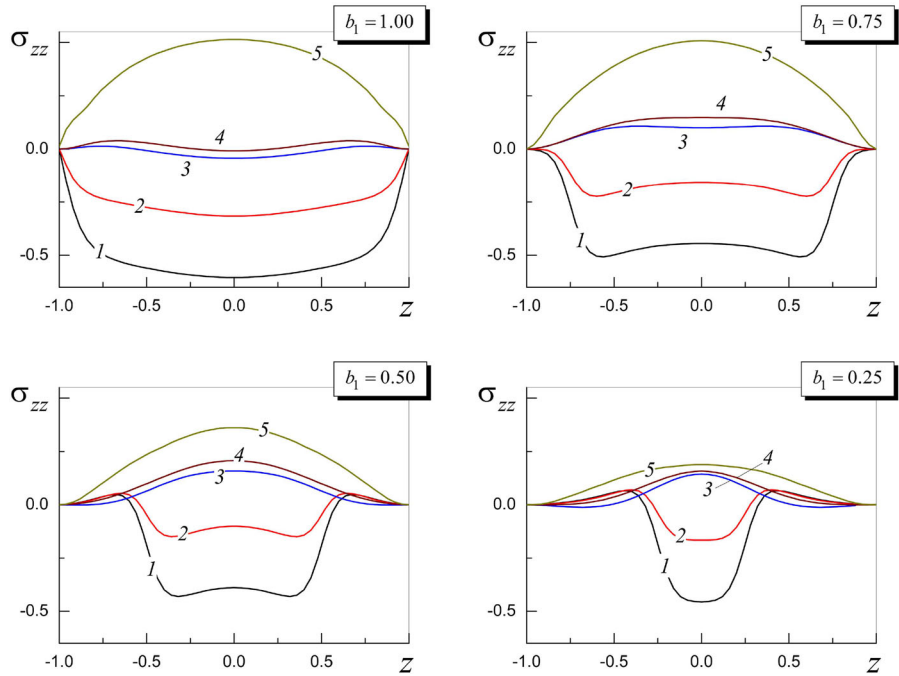


Fig. 3 The axial stress versus axial coordinate z at the specific radii $r = 0$ (curve 1), $r = 1/6$ (curve 2), $r = 1/2$ (curve 3), $r = 5/6$ (curve 4), and $r = 1$ (curve 5) of a “cubic” cylinder \mathcal{C} under the residual strains given by (26), where $e_1 = 1$, $e_2 = -1$, $r_1 = 1/3$, $r_2 = 2/3$, $b = 1$, $a_r = 18$, $a_z = 10$, and $b_1 = 1.00; 0.75; 0.50; 0.25$

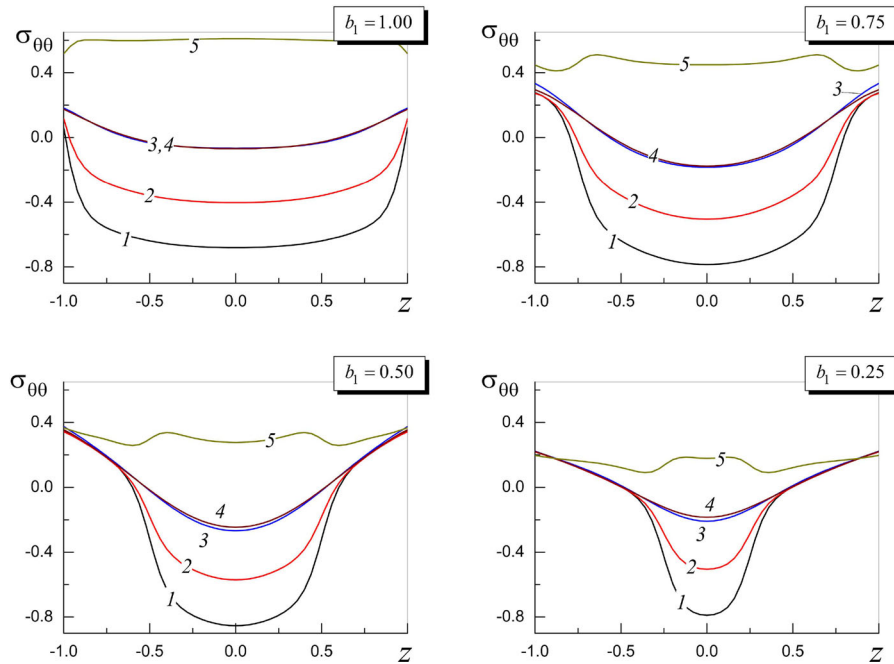


Fig. 4 The circumferential stress versus axial coordinate z at the specific radii $r = 0$ (curve 1), $r = 1/6$ (curve 2), $r = 1/2$ (curve 3), $r = 5/6$ (curve 4), and $r = 1$ (curve 5) of a “cubic” cylinder \mathcal{C} under the residual strains given by (26), where $e_1 = 1, e_2 = -1, r_1 = 1/3, r_2 = 2/3, b = 1, a_r = 18, a_z = 10$, and $b_1 = 1.00; 0.75; 0.50; 0.25$

stress depicted in Fig. 4. It is worth noting that the computed radial stress fits the necessary condition of the self-equilibration for the residual stress, i.e.,

$$\int_{-b}^b z\sigma_{rr}(r,z)dz = 0,$$

for all the values of the radial coordinate.

The axial stress in Fig. 3 exactly satisfies the boundary condition (2) on the end faces of the cylinder for all values of the radial coordinate. Similarly to the radial stress, the disturbance due to the residual strain (26) occupies almost entire length of the cylinder for greater values of b_1 , i.e., $b_1 = 1; 0.75$. This effect is well pronounced, in particular, on the lateral surface of the cylinder (curves 5), while the magnitude of this stress on the axis of the cylinder (curves 1) remains almost the same.

The tangential stress (Fig. 5) is an odd function of the longitudinal coordinate z satisfying the zero boundary conditions on both the lateral surface and end faces. For greater values of b_1 , this stress exhibits smaller maximum deviation from the zero distributions, which grows with narrowing the zone of the distributions of the residual strain (26).

Let us analyze the efficiency of the proposed computational algorithm with regard to solving the systems (25) by using the simple reduction method. The solution errors for the first and second disturbed problems depending on number of equations in the reduced systems (25) can be estimated with evaluating the corresponding functionalities calculated on the solution obtained for a selected value of N :

$$\delta_1 = \frac{\sqrt{\mathcal{F}_1^N}}{2}, \quad \delta_2 = \frac{\sqrt{\mathcal{F}_2^N}}{2}.$$

Here, \mathcal{F}_1^N and \mathcal{F}_2^N are the values of the functionals (22) and (23) calculated by solving the reduced systems obtained from (25) by keeping only N first equations. The results of evaluation conducted for $N = 5, 7, \dots 15$ are given in

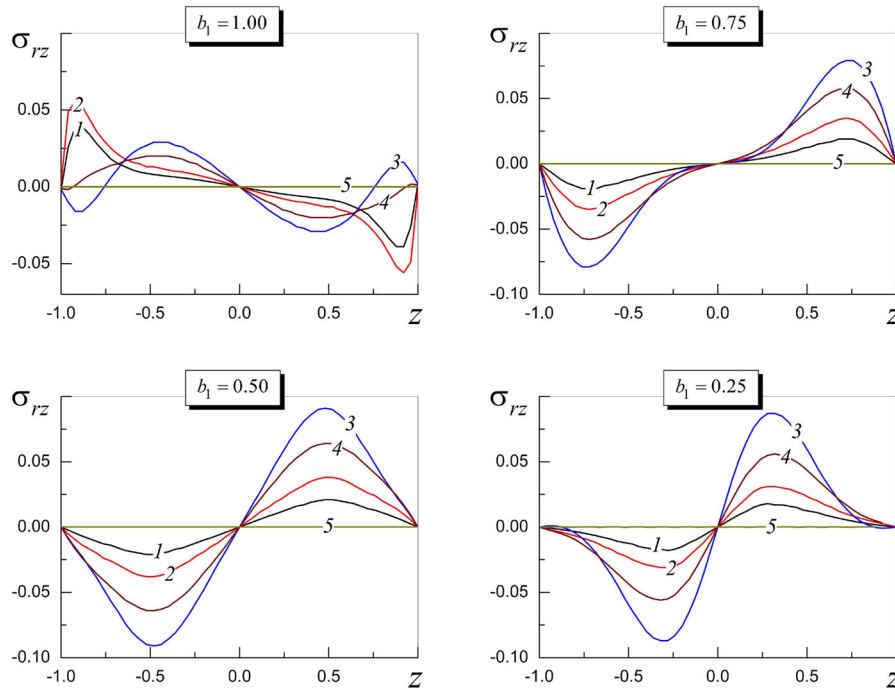


Fig. 5 The tangential stress versus axial coordinate z at the specific radii $r = 0$ (curve 1), $r = 1/6$ (curve 2), $r = 1/2$ (curve 3), $r = 5/6$ (curve 4), and $r = 1$ (curve 5) of a “cubic” cylinder \mathcal{C} under the residual strains given by (26), where $e_1 = 1, e_2 = -1, r_1 = 1/3, r_2 = 2/3, b = 1, a_r = 18, a_z = 10$, and $b_1 = 1.00; 0.75; 0.50; 0.25$

Table 1 The errors in the minimization functionals (22) and (23) when using the reduced systems of equations

N	5	7	9	11	13	15
δ_1	0.01807	0.01496	0.00801	0.00474	0.00317	0.00191
δ_2	0.00593	0.00363	0.00252	0.00167	0.00122	0.00088

Table 1. As we can see, the accuracy gradually grows for greater values of N . The convergence of the solutions depends on the type of boundary conditions. On the basis of conducted numerical experiments, we can conclude that accuracy sufficient for practical goals can be achieved at $N \geq 9$.

5 Conclusion

A technique for evaluating axisymmetric residual stresses in a finite-length solid cylinder is presented. The cylinder’s surface is assumed to be free of force loadings. The residual stresses are induced by incompatible strains represented by an isotropic tensor, whose impact is encountered via the model of conventional-plastic strains.

An analytical solution to this problem is constructed by superposing the solutions of three individual problems. The first problem implies determining the basic state for an infinitely long solid cylinder of the same radius, which undergoes the considered distribution profiles of the incompatible strains. In order to find an exact solution to this problem, an analytical technique was employed that is based upon the implementation of the Goodier–Papkovitch potential constructed through the complete Legendre elliptic integral of the first kind.

In order to compensate the stresses induced by the found stress field when “cutting” the original cylinder of finite length out of the infinitely long one, two auxiliary problems are considered. The solutions to these problems

are constructed by implementing the Love biharmonic stress function and the general scheme of the method of homogeneous solutions, i.e., the ones satisfying the zero boundary conditions on the segments of the cylinder boundary, represented by different families of coordinate surfaces. These two problems are solved with the use of the variational method, in which the subordination of the solution to the boundary conditions is performed in the norm L_2 . As a result, the problems are reduced to infinite systems of linear algebraic equations regarding the unknown complex coefficients. Because of the zero asymptotic of the coefficients, the obtained systems can be solved within any given accuracy by implementing the simple reduction method. This makes the obtained system to be advantageous over the ones obtained through the method of cross-wise superposition [33]. The conducted numerical experiments for the considered case studies confirm high convergence of the suggested algorithm, as sufficient accuracy is reached at $N \geq 9$.

The constructed solution allows for analyzing the residual stresses in the finite-length cylinders with different ratios and various nature of the incompatible strains. The solution can be efficiently extended for the analysis of thermal stresses by implying the incompatible strains to be the thermal ones, i.e., $\varepsilon_{ll}^0 = \alpha(T(r, z) - T_0(r, z))$, where $l = \{r, \theta, z\}$, α is the linear thermal expansion coefficient, $T_0(r, z)$ is the reference temperature of the stress-free cylinder, and $T(r, z)$ is the actual temperature.

Finally, in view of the fact that the solution is constructed in an analytical form, it can be rather advantageous for further implementation with the development of non-destructive evaluation techniques for the residual stresses in elastic cylinders of finite length.

Acknowledgements This paper is devoted to the brilliant memory of Prof. Vasyil Chekurin (1951–2021) whose life was taken by COVID-19 in the middle of his research into this subject.

Appendix A

Functions in expressions (19) for the stresses of the first disturbed problem:

$$\begin{aligned} \sigma_{rr,k}^{(1)}(r, z) &= 2\mu\gamma_k^2 \cosh(\gamma_k z) \left(\kappa_k ((1 - 2\nu)J_0(\gamma_k r) - r\gamma_k J_1(\gamma_k r)) + \frac{2}{\pi\gamma_k r} (r\gamma_k J_0(\gamma_k r) - J_1(\gamma_k r)) \right), \\ \sigma_{\theta\theta,k}^{(1)}(r, z) &= 2\mu\gamma_k \cosh(\gamma_k z) \left(\kappa_k (1 - 2\nu)\gamma_k J_0(\gamma_k r) + \frac{2}{\pi r} J_1(\gamma_k r) \right), \\ \sigma_{zz,k}^{(1)}(r, z) &= 2\mu\gamma_k^2 \cosh(\gamma_k z) \left(\kappa_k (\gamma_k r J_1(\gamma_k r) - 2(2 - \nu)J_0(\gamma_k r)) - \frac{2}{\pi} J_0(\gamma_k r) \right), \\ \sigma_{rz,k}^{(1)}(r, z) &= 2\mu\gamma_k^2 \sinh(\gamma_k z) \left(-\kappa_k (2(1 - \nu)J_1(\gamma_k r) + \gamma_k r J_0(\gamma_k r)) - \frac{2}{\pi} J_1(\gamma_k r) \right). \end{aligned}$$

Appendix B

Functions in expressions (21) for the stresses of the second disturbed problem:

$$\begin{aligned} \sigma_{rr,k}^{(2)}(r, z) &= 2\mu \left(\frac{\lambda_k}{r} (\lambda_k r (1 + 2\nu + \lambda_k \nu_k) J_0(\lambda_k r) - (1 + \lambda_k \nu_k) J_1(\lambda_k r)) \cosh(\lambda_k z) \right. \\ &\quad \left. + \lambda_k^2 z \left(\lambda_k J_0(\lambda_k r) - \frac{1}{r} J_1(\lambda_k r) \right) \sinh(\lambda_k z) \right), \\ \sigma_{\theta\theta,k}^{(2)}(r, z) &= 2\mu \frac{\lambda_k}{r} \left((2\nu\lambda_k r J_0(\lambda_k r) + (1 + \lambda_k \nu_k) J_1(\lambda_k r)) \cosh(\lambda_k z) + \lambda_k z J_1(\lambda_k r) \sinh(\lambda_k z) \right), \end{aligned}$$

$$\sigma_{zz,k}^{(2)}(r, z) = -2\mu\lambda_k^2 J_0(\lambda_k r) \left(\lambda_k z \sinh(\lambda_k z) - (1 - 2\nu - \lambda_k \nu_k) \cosh(\lambda_k z) \right),$$

$$\sigma_{rz,k}^{(2)}(r, z) = 2\mu\lambda_k^2 J_1(\lambda_k r) \left((2\nu + \lambda_k \nu_k) \sinh(\lambda_k z) + \lambda_k z \cosh(\lambda_k z) \right).$$

Appendix C

$$M_{mk}^{lp} = \frac{1}{2} \int_0^1 r \left(\sigma_{zz,k}^p(r) \sigma_{zz,m}^l(r) + \sigma_{rz,k}^p(r) \sigma_{rz,m}^l(r) \right) dr,$$

$$N_{mk}^{lp} = \frac{1}{2} \int_0^b \left(\sigma_{rr,k}^p(z) \sigma_{rr,m}^l(z) + \sigma_{rz,k}^p(z) \sigma_{rz,m}^l(z) \right) dz - \frac{1}{2b} \int_0^b \sigma_{rr,k}^p(z) dz \int_0^b \sigma_{rr,m}^l(z) dz,$$

$$K_m^l = - \int_0^1 r \left(\hat{\sigma}_{zz}(r, b) \sigma_{zz,m}^l(r) + \hat{\sigma}_{rz}(r, b) \sigma_{rz,m}^l(r) \right) dr,$$

$$L_m^l = - \int_0^b \left(\hat{\sigma}_{rr}(1, z) \sigma_{rr,m}^l(z) + \hat{\sigma}_{rz}(1, r) \sigma_{rz,m}^l(z) \right) dz - \frac{1}{b} \int_0^b \hat{\sigma}_{rr}(1, z) dz \int_0^b \sigma_{rr,m}^l(z) dz,$$

where

$$\sigma_{zz,\ell}^1(r) = \sigma_{zz,\ell}^{(1)}(r, b), \quad \sigma_{zz,\ell}^2(r) = \bar{\sigma}_{zz,\ell}^{(1)}(r, b),$$

$$\sigma_{rz,\ell}^1(r) = \sigma_{rz,\ell}^{(1)}(r, b), \quad \sigma_{rz,\ell}^2(r) = \bar{\sigma}_{rz,\ell}^{(1)}(r, b),$$

$$\sigma_{rr,\ell}^1(z) = \sigma_{rr,\ell}^{(2)}(1, z), \quad \sigma_{rr,\ell}^2(z) = \bar{\sigma}_{rr,\ell}^{(2)}(1, z),$$

$$\sigma_{rz,\ell}^1(z) = \sigma_{rz,\ell}^{(2)}(1, z), \quad \sigma_{rz,\ell}^2(z) = \bar{\sigma}_{rz,\ell}^{(2)}(1, z),$$

$$\ell = \{m, k\}, \quad m = 1, 2, \dots, \quad k = 1, 2, \dots, \quad p = 1, 2, \quad l = 1, 2.$$

References

1. Schajer GS, Ruud CO (2013) Overview of residual stresses and their measurement. In: Schajer GS (ed) Practical residual stress measurement methods. Wiley, New York, pp 1–28
2. Dong P, Brust FW (2000) Welding residual stresses and effects on fracture in pressure vessel and piping components: a millennium review and beyond. J Pres Ves Technol Trans ASME 122:329–338
3. Tsai CL, Kim DS (2005) Understanding residual stress and distortion in welds: an overview. In: Feng Z (ed) Processes and mechanisms of welding residual stress and distortion. Woodhead Pub. Ltd., Cambridge, pp 3–31
4. Łagoda T (2008) Lifetime estimation of welded joints. Springer, Berlin
5. Schajer GS, Whitehead PS (2013) Hole drilling and ring coring. In: Schajer GS (ed) Practical residual stress measurement methods. Wiley, New York, pp 29–64
6. Peng Y, Zhao J, Chen L, Dong J (2021) Residual stress measurement combining blind-hole drilling and digital image correlation approach. J Constr Steel Res 174:106346
7. Smith DJ (2013) Deep hole drilling. In: Schajer GS (ed) Practical residual stress measurement methods. Wiley, New York, pp 65–88
8. Attalla M, Kandil S, Gepreel MA-H, Daha MA (2022) Effect of employing buffer layer in repaired dissimilar welded joints on the residual stresses based on contour and slitting methods. J Manuf Process 73:454–462
9. Hill MR (2013) The slitting method. In: Schajer GS (ed) Practical residual stress measurement methods. Wiley, New York, pp 89–108
10. Prime MB, DeWald AT (2013) The contour method. In: Schajer GS (ed) Practical residual stress measurement methods. Wiley, New York, pp 109–138

11. Murray CE, Noyan IC (2013) Applied and residual stress determination using X-ray diffraction. In: Schajer GS (ed) Practical residual stress measurement methods. Wiley, New York, pp 139–162
12. Hollmann A, Meixner M, Klaus M, Genzel C (2021) Concepts for nondestructive and depth-resolved X-ray residual stress analysis in the near-surface region of nearly single crystalline materials with mosaic structure. *J Appl Crystallogr* 54:22–31
13. Holden TM (2013) Neutron diffraction. In: Schajer GS (ed) Practical residual stress measurement methods. Wiley, New York, pp 195–224
14. Buttle DJ (2013) Magnetic methods. In: Schajer GS (ed) Practical residual stress measurement methods. Wiley, New York, pp 225–258
15. Bray DE (2013) Ultrasonics. In: Schajer GS (ed) Practical residual stress measurement methods. Wiley, New York, pp 259–278
16. Nelson DV (2013) Optical methods. In: Schajer GS (ed) Practical residual stress measurement methods. Wiley, New York, pp 279–302
17. Berezhnyts'ka MP (2001) Methods for determining residual welding stresses and their relief (a review). *Mater Sci* 37(6):933–939
18. Dong P, Brust FW (2000) Welding residual stresses and effects on fracture in pressure vessel and piping components: a millennium review and beyond. *J Pres Ves Technol Trans ASME* 122(3):329–338
19. Osadchuk VA, Bazilevich LV (1997) A nondestructive numerical-experimental method of determining the residual stresses in welded shells of revolution. *J Math Sci* 86:2650–2652
20. Osadchuk VA, Kir'yan VI, Bazilevich IV (1998) The inverse conditionally correct problem of determining the residual stresses in compound welded shells of revolution. *J Math Sci* 88:437–441
21. Nowacki W (1966) Thermoelastic distortion problems. *Bull de l'Académie Polonaise des Sci* 14(3):213–223
22. Podstrigach YS, Osadchuk VA (1969) Determination of the stress state of thin shells taking into account strains due to physico-chemical phenomena. *Mater Sci* 4:160–165
23. Mura T (1987) Micromechanics of defects in solids. Martinus Nijhoff Pub, Dordrecht
24. Vihak VM, Tsymbalyuk LI, Shablii OM (2001) Distribution of residual stresses induced by axially symmetric plastic strains in a layer. *Mater Sci* 37(1):19–24
25. Osadchuk VA, Tsymbalyuk LI (2003) Distribution of residual stresses in a layer containing a welded cylindrical disk. *Mater Sci* 39(2):225–231
26. Tokovyy YV, Ma C-C (2011) Analysis of residual stresses in a long hollow cylinder. *Int J Press Ves Piping* 88:248–255
27. Osadchuk VA, Banakhevych YV, Ivanchuk OO (2006) Determination of the stressed state of main pipelines in the zones of circular welds. *Mater Sci* 42:256–262
28. Tokovyy YV, Ma C-C (2007) Analytical determination of residual stresses in a butt-weld of two thin rectangular plates. *Proc Appl Math Mech* 7(1):2090013–4
29. Vihak VM, Tokovyi YV (2002) Investigation of the plane stressed state in a rectangular domain. *Mater Sci* 38:230–237
30. Meleshko VV (2003) Selected topics in the history of the two-dimensional biharmonic problem. *Appl Mech Rev* 56(1):33–85
31. Tokovyy Y, Ma C-C (2021) The direct integration method for elastic analysis of nonhomogeneous solids. Cambridge Scholars Publishing, Newcastle
32. Yuzvyak M, Tokovyy Y, Yasinsky A (2021) Axisymmetric thermal stresses in an elastic hollow cylinder of finite length. *J Therm Stress* 44(3):359–376
33. Meleshko VV, Tokovyy YV, Barber JR (2011) Axially symmetric temperature stresses in an elastic isotropic cylinder of finite length. *J Math Sci* 176(5):646–669
34. Meleshko VV, Tokovyy YV (2013) Equilibrium of an elastic finite cylinder under axisymmetric discontinuous normal loadings. *J Eng Math* 78(1):143–166
35. Lurie SA, Vasiliev VV (1995) The biharmonic problem in the theory of elasticity. Gordon and Breach, Luxembourg
36. Chekurin VF, Postolaki LI (2009) Theoretical and experimental determination of residual stresses in plane joints. *Mater Sci* 45(2):318–328
37. Chekurin V, Postolaki L (2014) Problem of nondestructive evaluation of residual stresses in a pipeline according to the data of magnetoelastic measurements. *Fiz-Mat Model Inform Tekhnol* 20:218–228
38. Chekurin VF, Postolaki LI (2018) Residual stresses in a finite cylinder. Direct and inverse problems and their solving using the variational method of homogeneous solutions. *Math Model Comput* 5(2):119–133
39. Chekurin VF, Postolaki LI (2020) Application of the variational method of homogeneous solutions for the determination of axisymmetric residual stresses in a finite cylinder. *J Math Sci* 249:539–552
40. Reza Eslami M, Hetnarski RB, Ignaczak J, Noda N, Sumi N, Yo Tanigawa (2013) Theory of elasticity and thermal stresses. Explanations, problems and solutions. Springer, Dordrecht
41. Sadd MH (2014) Elasticity. Theory, applications, and numerics. Elsevier, Amsterdam
42. Papkovitch PF (1937) General integral of thermal stresses (on the work 'Thermal stresses in the theory of elasticity' by N. N. Lebedev). *Prikl Mat Mekh* 1(2):245–246
43. Goodier JN (1937) On the integration of the thermo-elastic equations. *Philos Mag (Ser 7)* 23:1017–1032
44. Ang W-T, Ooi E-H (2008) A dual-reciprocity boundary element approach for solving axisymmetric heat equation subject to specification of energy. *Eng Anal Bound Elem* 32(3):210–215
45. Love AEH (1927) A treatise on the mathematical theory of elasticity. Cambridge University Press, Cambridge
46. Chekurin V, Postolaki L (2016) Application of the least squares method in axisymmetric biharmonic problems. *Math Probl Eng* 2016:3457649

47. Lurie AI (2005) Theory of elasticity. Springer, Berlin
48. Kantorovich IV, Krylov VI (1958) Approximate methods of higher analysis. Interscience Publishers, New York

Publisher's Note Springer Nature remains neutral with regard to jurisdictional claims in published maps and institutional affiliations.